On the Frequency Dependence of the PDIV in Twisted Pair Magnet Wire Analogy in Dry Air

Author(s):
Sefl, Ondrej; Färber, Raphael; Franck, Christian

Publication date:
2023-10

Permanent link:
https://doi.org/10.3929/ethz-b-000610475

Originally published in:
IEEE Transactions on Dielectrics and Electrical Insulation 30(5), https://doi.org/10.1109/tdei.2023.3272300

On the Frequency Dependence of the PDIV in Twisted Pair Magnet Wire Analogy in Dry Air

Ondřej Šefl, Raphael Färber, and Christian M. Franck, *Senior Member, IEEE*

***Abstract*— This paper presents an experimental verification of a PDIV model for twisted-pair magnet wires (TPMW). The model is physically rooted in an inception criterion based on secondary electron feedback and parametrizes the PDIV of wedge-shaped gas gaps (such as TPMW) solely in terms of its reduced coating thickness—the ratio of coating thickness to its relative permittivity. According to the literature, the coating's permittivity and thickness should play a significant role in determining the PDIV. Still, no explicit quantification of their concurrent effects is often given, and they are frequently treated as decoupled parameters. Therefore, extensive measurements of PDIV of samples analogous to TPMW coated with dielectric materials of different permittivity (sealed and unsealed alumina, silicone polyester, and perfluoroalkoxy alkane) and thickness (≈45 to 80 µm) are performed. The PDIV of the test samples is determined under sinusoidal test voltage in the frequency between 10 to 60 000 Hz. It is shown that the PDIV can be predicted based on the relative permittivity and thickness of the coating, and the frequency dependence is due only to the change of permittivity with frequency. Temperature and pressure are kept approximately constant at their ambient values (ca. 23 ℃ & 970 mbar), and only dry air is used to exclude the effect of humidity on the insulation's permittivity. Ultimately, the role of surface charge is discussed qualitatively by comparing the PDIV with the partial discharge extinction voltage (PDEV) and their repetitive counterparts (RPDIV, RPDEV).**

***Index Terms*— PDIV, twisted-pair magnet wires, relative permittivity, reduced coating thickness, wedge-shape geometry, frequency, gas breakdown model**

I. Introduction

DUE to the rising demand for electric vehicles and the tendency to further electrify airplanes (more electric aircraft), a substantial effort is exerted toward optimizing the employed electric drives. These are, above all, induction motors driven by PWM-regulated inverters, which frequently use magnet wires (TPMW are their mock-ups for test purposes) as stator windings. Since an integral part of the design optimization process is the minimization of the insulation system within the respective reliability margins, determining the reliability with respect to degradation processes is crucial.

The partial discharge (PD) phenomenon is generally accepted as the main factor determining the degradation, hence the reliability [1], [2]. For organic materials (Type I), the PDs can result in the failure of the insulation system within very short times [3]. For this reason, determining and predicting the voltage at which the PDs incept (PDIV) is pivotal. Especially regarding the PWM regulation, the influence of excitation voltage frequency needs to be understood.

Wada *et al.* investigated the PDIV of wedge-shaped air gaps with a PE and PVC insulation foil placed in between the electrodes in [4]. The PDIV was measured under AC voltage at 60, 1000 and 10 000 Hz, and the observed frequency dependencies were linked to the change in relative permittivity of the foil due to the frequency. In [5], Meyer et al. also investigated the influence of excitation voltage frequency on the PDIV, but this time under repetitive impulses. It was shown that increasing (impulse) carrier waveform frequency reduces the repetitive PDIV in the range 5 kHz to 200 kHz. The authors speculated that the behavior cannot be linked to the measured change in relative permittivity and that it is instead connected to the overshoots of the waveforms, during which an overvoltage (in regard to the PDIV) was present for a longer total time as the carrier frequencies increased. Nevertheless, the work also reinterpreted the findings of Pfeiffer and Paede in [6] by connecting the observed PDIV trends (AC frequency 100 kHz to 3000 kHz) of enameled wires again to the change in relative permittivity of the enamel.

A similar inconsistency also prevails in works concerned with the physical modeling of the critical threshold (PDIV) of breakdown in the air gap of TPMW. In [7], Hayakawa *et al.* employed the volume-time theory to predict the PDIV under inverter stresses. Regardless of the investigated waveform, the critical field threshold was calculated from Schumann's criterion, whose 'streamer constant' value K was not given. Conversely, the K is provided in a later breakdown model [8], but its value is determined retrospectively from experimental data. In both models, the field in the air gap(s) between the TPMW is calculated from electrostatics, directly connecting it to the geometry (coating thickness s) and permittivity of the system parts. Unfortunately, due to the unknown/empiric nature of establishing the K constant and decoupling of the relative permittivity and thickness of the coating, their mutual connection to the PDIV cannot be drawn clearly.

The unclear or contradicting role of excitation voltage frequency on the PDIV in experimental and simulation works stipulated the analysis of the phenomenon performed in this work. Specifically, the emphasis is put on the role of the coating's permittivity and thickness (as highlighted in the literature), while the role of the other influencing factors

Ondřej Šefl, Raphael Färber, and Christian M. Franck are with the High Voltage Laboratory, ETH Zürich (email: sefl@eeh.ee.ethz.ch; raphael.faerber@eeh.ee.ethz.ch; franck@eeh.ee.ethz.ch

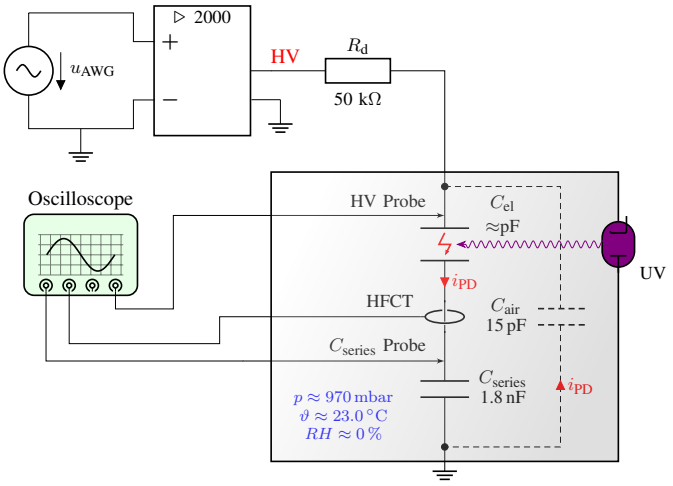

Fig. 1. Circuit diagram of the test setup. AWG: arbitrary waveform generator; R_d: decoupling resistor (filter); C_{el}: capacitance of the electrode pair; C_{series}: series capacitor (PD instrument); HFCT: high-frequency current transformer; UV: ultraviolet lamp

TABLE I
OVERVIEW OF THE TEST SETUP CAPABILITIES

Waveform amplitude	−20 kV to 20 kV (DC) 20 kV (peak; AC $\leq$ 10 kHz) 2 kV (peak; AC $\leq$ 60 kHz)
Waveform frequency	0 to 60 kHz
Waveform shape	Arbitrary within the above limitations
PD detection methods	Series capacitor (C_{series}) High-frequency current transformer (HFCT)

(temperature, pressure, humidity) is excluded. The problem is simplified by employing electrodes of a precise geometry to represent TPMW. These electrodes are coated with various dielectric materials, which all have a different relative permittivity and thickness so that an extensive set of (ε_r, s, PDIV) data is available for analysis using a breakdown model. The PDIV is measured over a broad range of frequencies, and it is shown that the model correctly predicts the PDIV when the frequency dependence of the permittivity is considered.

Structurally, this paper is divided into six sections. Following the Introduction in Section I, Section II describes the test setup employed in the investigation, focusing on the specific PD instruments intended for higher test voltage frequencies and the shape and material of the examined electrodes (test samples). The specification of the observed parameters and the course of action for the determination of the PDIV and other parameters are also given. Next, Section III briefly describes the model employed for predicting the PDIV. Section IV then presents the experimental results obtained for the different electrode materials over the employed range of test voltage frequencies and the model predictions. These results are then discussed in Section V. Ultimately, conclusions are drawn, and outlooks are mentioned in Section VI.

II. MATERIALS & METHODS

A. Test setup

A specialized test setup for investigating PDs under mixed-frequency / inverter medium-voltage (MFMV) stresses was built at the High Voltage Laboratory of ETH Zürich. The respective parts and devices employed for this paper are depicted in the circuit diagram in Figure 1. The test voltage is generated via an arbitrary wave generator connected to a power amplifier with an amplification factor of 2000. The amplifier's output voltage (=test voltage) is then connected via a high-voltage cable and decoupling resistor to the test cell. Since the test cell is envisaged to be employed at various atmospheric conditions, the test samples are placed inside an enclosable steel vessel. The voltage stress is applied to it via a feed-through. In this work, the temperature and pressure were at their room values, and the relative humidity was kept at 0 % (dry air). Regarding the equipment, the test cell is installed with two different PD sensors, an ultraviolet light source, and humidity, temperature, and pressure sensors. An overview of the setup's voltage generation capabilities and the available PD detection methods are given in Table I.

The two PD instruments were specifically chosen as they are practically unaffected by the test voltage up to (and above) the employed power amplifier's upper-frequency limit (60 kHz). The series capacitor detection method was inspired by the works of Kimura et al. and Fukunaga et al. in [9] and [10], respectively, and is also listed as a suitable PD instrument in the IEC TS 61934:2011 standard. Fundamentally, the instrument operates as a voltage divider of the test voltage, and whenever a PD occurs, its transferred charge (magnitude) manifests as a very fast voltage jump superposed on the original signal. Thanks to the relatively large time constant of the instrument's discharge circuit (given by the 1.8 nF capacitance of the C_{series}-capacitor and the 10 MΩ input resistance of the voltage probe), the PD-induced voltage change decays slowly and can be easily observed via electronic test equipment even at low sampling frequencies.

During the experiment, a TiePie WS6 DIFF-1000XMG oscilloscope was employed to measure the PD signals and test voltage. Additionally, a TiePie WiFiScope WS5-540X was used to generate the excitation voltage for the power amplifier. Both oscilloscopes and the temperature, pressure, and humidity sensors were connected to a PC via Ethernet-optical fiber-Ethernet links. This way, the test setup could be operated with a full galvanic decoupling, and all the relevant data could be read and collected from a single access point.

Lastly, due to the absence of humidity, there was a concern regarding a possibly too large statistical time lag during the measurements, as highlighted in [11] and [12]. Hence, a cold-cathode, mercury-vapor, low-pressure germicidal UV lamp was added to the setup to generate free electrons from the test samples' surface via the photoelectric effect when needed. Its spectrum has significant peaks at 185 nm and 254 nm, with an estimated respective output power of about 0.1 W at the latter wavelength. The lamp was situated in a housing mountable on the test cell. Such a solution provided two main advantages—the cooling of the UV lamp took place outside the test cell, hence not influencing the internal temperature, while at the same time, electromagnetic interference with the PD instruments was suppressed. The lamp was separated from the test cell by a vacuum-tight, UV-transmissible window to isolate the test cell atmosphere from the external one.

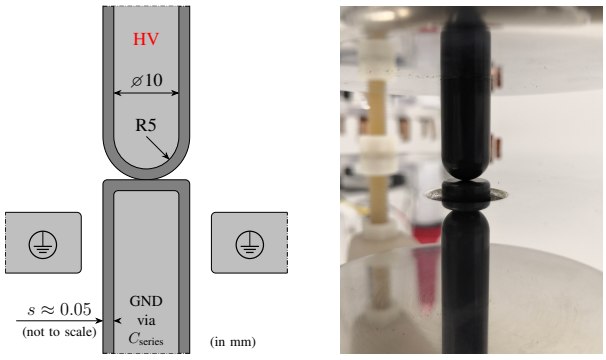

Fig. 2. (a) Schematic cross-section of the used electrode geometry; (b) placement of the actual electrodes within the test cell (note that the electrodes are also reflected on the surface of the electrode fixture body).

TABLE II
MEASURED COATING THICKNESS OF THE EMPLOYED ELECTRODES

Coating material	Abbreviation	Coating thickness (lower / upper* electrode) in µm
Unsealed alumina	UA	(46.5 ± 3.0) / (47 ± 5)
Silicone polyester	SiPo	(55.0 ± 2.0) / (45 ± 5)
Sealed alumina	SA	(48.1 ± 2.2) / (48 ± 6)
Perfluoroalkoxy alkane	PFA	(74.0 ± 2.3) / (85 ± 7)

* The larger uncertainty is a result of the rather small rounding radius of the upper electrode, which substantially enlarged the coating thickness readings and hence their absolute scattering. The actual thickness was determined by subtracting the reading obtained for an uncoated calibration electrode of a similar shape.

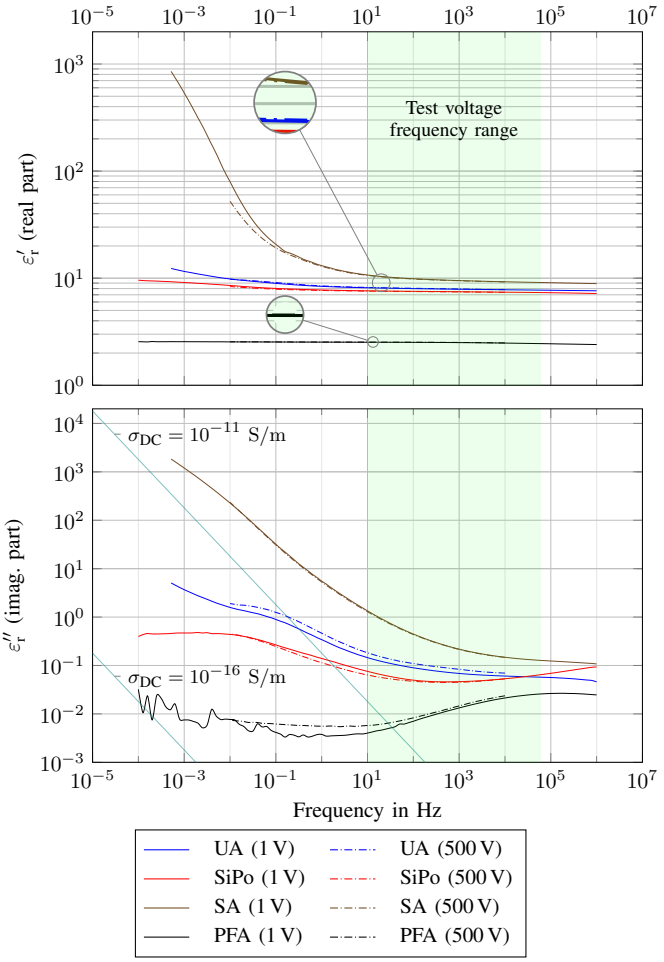

Fig. 3. Dependence of the real and imaginary part of the electrode coating materials' relative permittivity on voltage frequency. The highlighted frequency range (green) corresponds to the range of test voltage frequencies employed in the experiment. Note that virtually no difference between the permittivity measured at 1 V and 500 V (both RMS) was determined (magnified circles in the upper diagram), meaning that the parameter is expected to be voltage-independent in the range of the employed test voltage amplitudes. In the lower diagram, two lines corresponding to different values of DC conductivity σ_{DC} are plotted. For low enough frequencies, the steepness of the ε_r''-trends should become identical to those of these lines, as $\sigma_{DC} = \lim_{f \to 0} (\varepsilon_r''(f) / (2\pi f))$ from $\varepsilon_r''(f) = \sigma(f) / (2\pi f)$. By this logic, it can be shown that the (DC) conductivity of a material is at least as small as the threshold delimited by the given 'conductivity' line.

B. Test samples (wedge-shaped gas gaps)

The investigated test samples consisted of a pair of electrodes with a uniform dielectric coating. A schematic depiction of the electrodes' cross-section and dimensions are given in Figure 2a. Figure 2b depicts an actual electrode pair installed in the test setup. The use of a flat lower electrode instead of a half-spherical one substantially facilitated the correct placement of the electrode pair. At the same time, the electrode arrangement still maintained the fundamental characteristics of the reference TPMW (quasi-uniform field in between coated conductors, broad range of air gap distances) whilst providing exact control of the geometry, and therefore eliminating one uncertainty factor. The representability of the samples to TPMW is justified by the presence of a uniform electric field in between the electrodes, as shown by the FEM-simulated electric field lines depicted in Figure 6.

Four such electrode pairs with different dielectric coating materials were used during the experiment, namely alumina (Al_2O_3) left with its pores unsealed ("unsealed alumina" = UA), alumina with its pores sealed in boiling water ("sealed alumina" = SA), silicone polyester (SiPo), and perfluoroalkoxy alkane (PFA). The coating thickness of the individual electrodes, measured with an eddy current coating thickness gauge, is listed in Table II.

The dielectric properties of each coating material were determined by dielectric spectroscopy performed between 1×10^{-4} Hz to 1×10^{6} Hz at 1 V (RMS) with a Novocontrol Technologies Alpha-A modular measurement system. Figure 3a and b show, respectively, the real and imaginary parts of the coating's relative permittivity. Note that the coatings were also characterized at 500 V (RMS) over a reduced frequency range to confirm that the values of relative permittivity are not significantly voltage-dependent (non-linear).

C. Observed parameters

At first, the HFCT was employed to detect the onset of the first discharge(s), as its PD output signal could be easily used for triggering (PD manifested as impulses clearly above the noise floor). Nevertheless, it was observed for all measurements that the amplitudes of even the weakest PDs (at PDIV) were already large enough to be reliably detectable

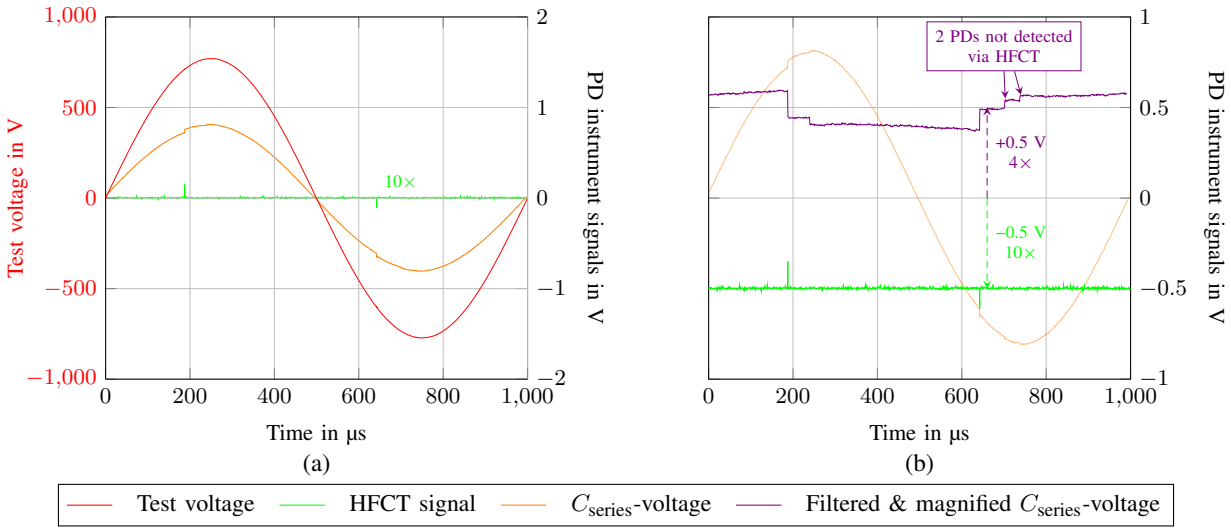

Fig. 4. (a) Signals from the HV probe and the two PD instruments over a single period at a test voltage slightly above the PDIV (voltage frequency 1 kHz, 100 MSa/s, 1000 Sa (down-sampled), HFCT tenfold magnified). (b) Detail of the PD instrument signals: the purple trend was obtained by subtracting a suitable fraction of the test voltage signal from the phase-adjusted C_{series}-signal to suppress the sinewave (plotted with an offset of +0.5V and fourfold magnification).

via the C_{series}-method. Hence, owing to this method's lower requirements on the signal sampling rate, the C_{series}-sensor was employed as the reference PD instrument. This feature was crucial in the evaluation of the repetitivity of the PDs at lower test voltage frequencies, as the HFCT's signal requires sufficient sampling rate to reliably indicate that a PD occurred. For the employed oscilloscope, it was determined that a sampling rate of 50 MSa/s, paired with the devices' integrated peak detect (glitch capture) function, was adequate to indicate a PD in >95 % of the cases, which was deemed reliable regarding the chosen measurement procedure (section II-D). Such a sampling rate meant that, for instance, at a test voltage frequency of 10 Hz, the HFCT would have required at least 5 MSa to reliably indicate possible PDs over just one period. To handle such large amounts of data would substantially slow down the evaluation of the PD activity and respectively prolong the measurements.

Figure 4a shows example voltage signals obtained from the HV probe and both PD instruments at a voltage slightly above the PDIV. The details of the PD instrument signals as well as the post-processed signal from the C_{series} instrument are depicted in 4b. Such post-processing increased the sensitivity of the C_{series} instrument over the HFCT, as seen from the detection of the latter two PD signals of the second halfwave. Also note that the PDs occurred only in the first halves of both halfwaves, which suggests that surface charges strongly affect the PDs after inception. This topic is further discussed in Section V-B.

While PDIV was the main focus of the paper, the other PD-related parameters, namely the PD extinction voltage (PDEV) and both parameters' repetitive variants, RPDIV and RPDEV, were also determined to quantify the surface charge effect. Regarding the RPDIV, whenever the PD activity started to appear repetitive, five random oscillograms of at least five periods were taken and evaluated. If in at least half of them PDs were present in 50 % or more halfwaves, the test voltage was labeled as the RPDIV. If not, the test voltage was increased and the process repeated. As soon as the RPDIV was determined, the test voltage was further increased to reach continuous PD activity (at least one PD occurring in 90 % of the halfwaves). Then, the voltage was gradually reduced, in steps specified in section II-D. The oscillograms started to be analyzed as soon as the discharge activity appeared to be discontinuous and if in five random oscillograms PDs occurred in less than 50 % of the halfwaves, the test voltage was labeled as RPDEV. The last remaining parameter, PDEV, was established when no discharges were observed via the PD instrument over the entire evaluation period (defined in the next section).

D. Measurement procedure

The initial step, prior to any measurement series, was the conditioning of the air inside the test cell. As the (ambient) temperature and pressure varied only little (ca. ±0.5 °C and ±10 mbar), respective changes in the PDIV were expected to be negligible (Fig. 6 in [12] and Fig. 17 in [1]). As for the relative humidity, it was brought down to ≈0 % by flushing the test cell with dry air. To ensure that moisture content inside the dielectric coatings would be negligible as well, the electrodes had been kept in an oven (50 °C, constantly flushed with dry air to ensure a RH of ≈0 %) for several days prior to their deployment. Additionally, after the electrodes were mounted, the test cell was conditioned with dry air for at least 24 h.

The PDIV measurement then took place: in each series, the four PD voltage parameters (PDIV, RPDIV, PDEV, RPDEV) were measured for a total of 35 different frequencies of the sinusoidal test voltage. These were evenly spaced on a logarithmic axis spanning the operation frequency range of the voltage source (10 Hz to 60 000 Hz). The measurement order was always randomized so that possible temporal changes of the test samples could be easily spotted and not misattributed

as an effect of the test voltage frequency. Concerning the choice of the initial test voltage, the PDIV was first estimated at 100 Hz under the artificial UV illumination, as the value would have been be close to the expected minimum PDIV (the coating's permittivity was almost at its maximum for the employed frequency range), while the test frequency was deemed sufficiently high to promote PD activity quick enough with respect to the voltage rise protocol. A voltage rise rate of $20\,\mathrm{V\,s^{-1}}$ (peak) was employed to roughly estimate the PDIV (following the PDIV definition per section II-B). As soon as the "PDIV" was reached, its value was noted and the initial test voltage was established at 100 V (peak) below it. The test voltage was then turned off, its frequency changed to the first test value, and applied again. The voltage was increased (in a non-specific manner) to the newly-defined initial value and then observed for 30 s to ensure no PD activity ensues. From there, it was gradually increased by ca. 0.5 % of the initial voltage every 5 s. During this time, the PD instrument signals were observed, and if the criteria defined in Section II-C were met, the corresponding PD voltage parameters were recorded. When establishing the RPDEV and PDEV, the voltage was reduced in analogous steps, i.e., by ca. 0.5 % of the initial voltage every 5 s. When all the PD voltage parameters were determined, the test voltage was turned off and its frequency was changed according to the measurement plan. The process was then repeated for the remaining test frequencies. At the end of the measurement, it was verified that the PDIV is stable (no significant degradation of the coating has occurred) by repeating the measurements at the first few test frequencies.

During the experiment, it was observed that the (R)PDIV values substantially scattered for certain combinations of materials and frequencies, suggesting that the statistical time lag influenced the measured PDIV. This claim was further supported by the observations from measurements at low RH in both [11] and [12]. Since the *minimum* PDIV was regarded as the key parameter (both in regard to the accompanying breakdown model and reliability point of view), artificial UV illumination was employed to promote the availability of free electrons, presumably via photoemission from the dielectric surfaces. This allows PDs to incept closer to the minimum inception threshold for a given (average) rate of rise of the test voltage. The differences between the PDIV values obtained following the same voltage protocol, once with and once without the artificial UV illumination, are depicted in Figure 5.

It should be noted that a substantial scattering of the PFA-coated electrode pair's PDIV was observed even under UV illumination. This behavior was attributed to the specific dielectric properties of the material as discussed in Section V-B. Qualitatively this can be seen later in Figure 8, where the PFA electrodes are shown to have the highest disparity between PDIV and PDEV, which is a marker of the effect of surface charges on the repetitive PD activity. During the measurement of the PFA coating, a very weak PD signal (detectable only via magnified C_{series}-signal) could be observed even at around PDEV if not enough time between the successive measurements was given (residual surface charge not dissipated). These discharges then quickly developed into much stronger discharge activity, already detectable via the

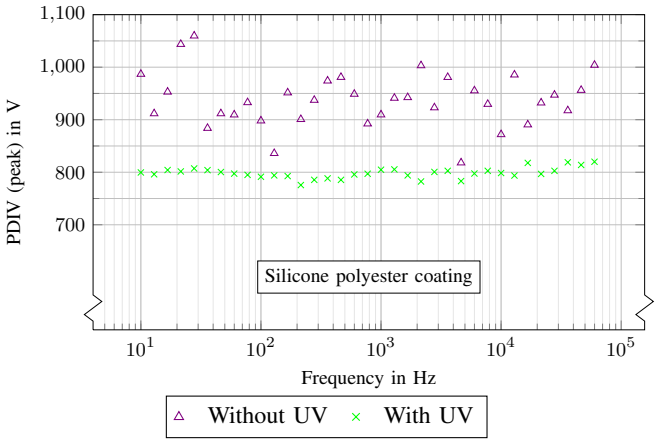

Fig. 5. Comparison of the PDIV measured for the silicone polyester electrode pair under different types of artificial UV illumination.

HFCT. The issue was resolved by starting the individual measurements after a pause of 120 s at a voltage ≈100 V below the PDEV, allowing the surface charge to dissipate sufficiently. Even though the scattering was still large, the obtained PDIVs were similar to the first-ever measured PDIV and were hence deemed "correct" in the sense of applying to surface-charge-free initial conditions (as assumed in the model).

III. PDIV MODELLING

The PDIV is modeled as the lowest electrode voltage U_{el} at which the voltage U_{g} across the air gap along any electric field line exceeds the breakdown voltage $U_{\mathrm{b}}(d)$ of a corresponding uniform air gap, where d is the field line length. The breakdown voltage of uniform air gaps as a function of the gap distance $10\,\mu\mathrm{m} \leq d \leq 10\,\mathrm{cm}$ is parametrized on the basis of measured data referenced in [13]–[15] and reads

$$U_{\mathrm{b}}(d) = (d/1\,\mathrm{m}) \cdot e^{f(\ln(d/1\,\mathrm{m}))}\,\mathrm{V}, \tag{1}$$

where f is the polynomial

$$\begin{aligned} f(x) =& 1.460 \times 10^{-1} - 1.245 \times 10^{-1} \cdot x \\ &- 2.304 \times 10^{-2} \cdot x^2 - 2.935 \times 10^{-3} \cdot x^3 \end{aligned} \tag{2}$$

The voltage across the gas gap having a field line length d in the gap can be obtained by employing a uniform approximation of the electrical field to calculate the voltage partition into the gas (U_{g}) and the dielectric coating ($U_{\mathrm{el}} - U_{\mathrm{g}}$):

$$U_{\mathrm{g}}(s/\varepsilon_{\mathrm{r}}', d) \approx \frac{U_{\mathrm{el}}}{1 + \frac{2}{d} \cdot \frac{s}{\varepsilon_{\mathrm{r}}'}}. \tag{3}$$

The approximation $\varepsilon_{\mathrm{r}}'' \ll \varepsilon_{\mathrm{r}}'$ used in the previous equation assumes low-loss dielectric materials and applies to the materials, ambient conditions, and frequency range used in this study (see Figure 3).

Defining the PDIV as the lowest electrode voltage for which the gas gap voltage exceeds the breakdown strength U_{b} of air somewhere in the wedge-shaped gas gap leads to the following parametrization of the PDIV:

$$\mathrm{PDIV}(s/\varepsilon_{\mathrm{r}}') \approx \min_{d \in (0,\infty)} U_{\mathrm{b}}(d) \cdot \left(1 + \frac{2}{d} \cdot \frac{s}{\varepsilon_{\mathrm{r}}'}\right). \tag{4}$$

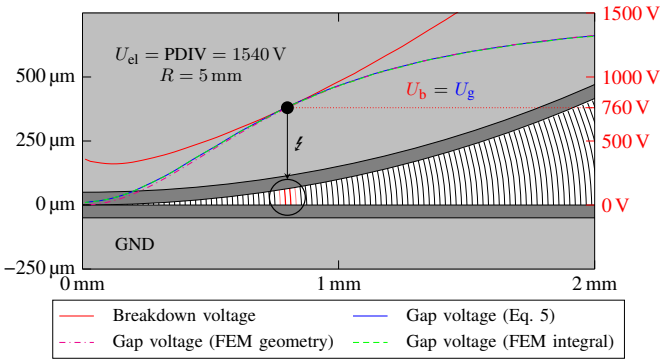

Fig. 6. FEM-simulated electric field lines in the air between the electrodes at a test voltage of 1540 V, which corresponds to the PDIV because $U_g = U_b$ is reached at the indicated location (around $x \approx 0.8$ mm). If a seed electron is available within the area, a PD will occur. The field appears quasi-uniform, implying that the wedge-shaped air gap can be split into a parallel connection of uniform gaps. For each field line, the 'local' gap voltage is estimated by Eq. (3) with the field line length given by Eq. (5), as well as the actual length extracted from the FEM simulation (FEM geometry). Finally, the gap voltage as extracted from the FEM simulation is also shown to validate the employed approximation (FEM integral).

The resulting parametrization of PDIV(s/ε_r') according to Equation (4) is shown in Figure 9.

An approximate location of the PD on the horizontal x-axis can be obtained by approximating the field line length at position x geometrically as a vertical line between the insulating surfaces, leading to

$$d(x) = \frac{x^2}{2 \cdot (R + s)}. \tag{5}$$

The breakdown voltages as well as the gap voltages calculated by the approximations (3) and (5) are shown in Figure 6. Moreover, in order to validate the approximations used above, the gap voltage is additionally shown as calculated by a full FEM simulation (integration of the electrical field along a field line, "integral") as well as Equation (3) in combination with the field line length extracted from the FEM simulation ("FEM geometry").

IV. Results

A. Comparison of the measured and simulated PDIV

The PDIV measured at various voltage frequencies is shown in Figure 7 for all four electrode coating materials (data points). All values were obtained under artificial UV illumination so that their scattering would be minimized (Section II-D). Interestingly, a relatively larger scatter was observed with the PFA polymer coating even in the presence of UV light, as emphasized in Section II-D.

The continuous lines represent the minimum PDIV for the given test voltage frequency predicted by the accompanying PDIV model described in Section III. Overall, the figure illustrates that each material's measured PDIVs match (mean relative error <5 %) the respective trends and absolute values of the PDIV model well . The measured PDIVs were almost in all cases slightly above the corresponding modeled critical thresholds, as expected due to the 'minimum' character of

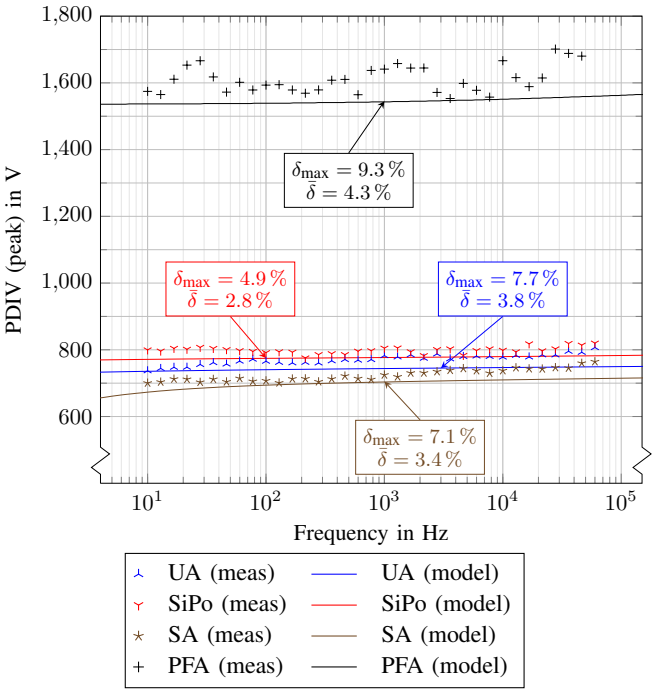

Fig. 7. Dependence of the measured (data points) and simulated (curves) values of PDIV on test voltage frequency for all four coating materials. Maximum and mean relative errors between the modeled and measured PDIV values, δ_{max} and $\bar{\delta}$, respectively, are given as well.

the modeled PDIV. Of note is also the substantial difference between the PDIVs of the PFA coating compared to the others, which stems primarily from the material's much lower relative permittivity, as highlighted in Figure 3.

B. Differences between PDIV and PDEV

To quantitatively investigate the effect of surface charge on the PD behavior of the investigated coating materials, each material's PDIV, PDEV, RPDIV, and RPDEV, measured according to Section II-C, were compared with each other. The trends of the PDIV/PDEV, RPDIV/PDIV, and RPDEV/PDEV ratios versus frequency are plotted in Figure 8 for all four materials.

Regarding the PDIV/PDEV ratio, Figure 8a illustrates that the smallest differences were obtained for sealed alumina, for which the PDIV was larger than the PDEV by just a few percent on average. The difference was slightly larger for both unsealed alumina and silicone polyester at around ≈10 %. Despite significant scattering, the PFA-coated electrodes showed the largest difference between the PDIV and PDEV for virtually all frequencies with the maximum observed increase being ≈25 %.

On the other hand, virtually no differences between RPDIV and PDIV were seen for any material, as depicted in Figure 8b. Ultimately, Figure 8c shows that the transition from a repetitive PD activity to a PD-free state (RPDEV/PDEV) was very abrupt for unsealed alumina at the majority of the investigated test voltage frequencies. Minimal differences between RPDEV and PDEV were observed for the sealed alumina coating, whereas they were most pronounced for the silicone polyester and PFA coatings.

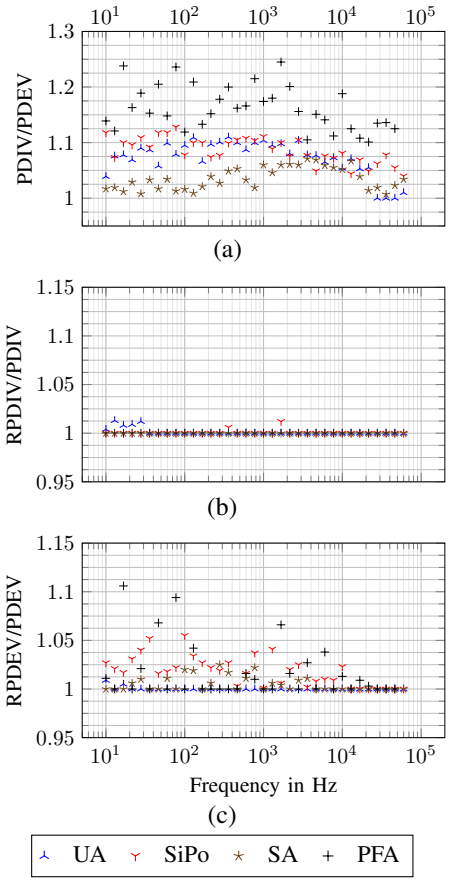

Fig. 8. Comparison of the ratios between the PDIV and PDEV and their repetitive counterparts for the four coating materials.

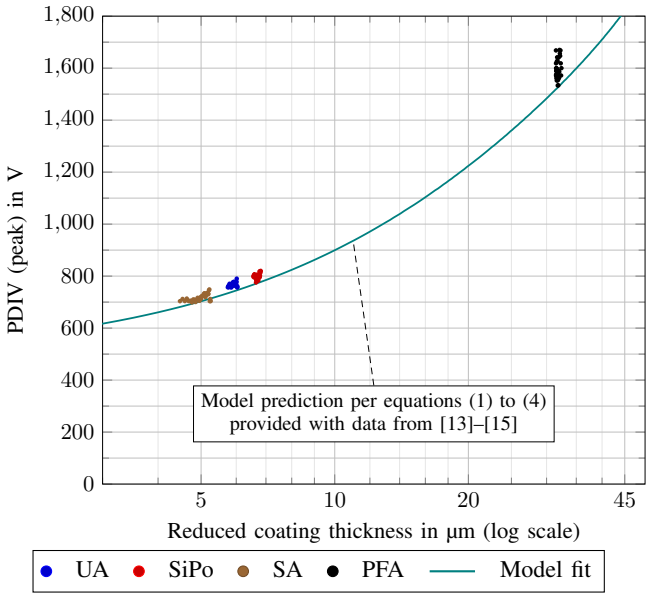

Fig. 9. Measured PDIV data points plotted against reduced coating thickness. The individual s/ε_r values were calculated from the data in Figure 3 and Table II. The solid line represents the minimum PDIVs predicted from the breakdown model in the reduced coating thickness range from 1 µm to 50 µm.

V. Discussion

A. Influence of the excitation voltage frequency on the PDIV

The main goal of this work is to clarify the frequency-dependence of the PDIV in a twisted-pair magnet wire insulation system analogy, in which the geometrical uncertainties could be largely eliminated. The results strongly support the conclusion that—under the examined environmental conditions—there is no inherent frequency dependence of the PDIV beyond its indirect effect via the frequency-dependence of the dielectric permittivity. Such a conclusion is in agreement with Wada *et al.* in [4]. In addition, the employed model also provides an accurate quantitative prediction of PDIV (the predictions of [4] were off by $\approx 20\,\%$).

It needs to be reiterated that the experimental data were obtained at room temperature, ambient pressure, and in dry air only. These environmental factors could change the PD ignition dynamics, and further measurements are required to extend the above conclusion to other conditions.

Moreover, it was observed that surface charge deposited via previous PDs could substantially reduce the PDIV for long periods after the PD activity ceases (PFA measurements comment in Section II-D). Presently, the accompanying model does not take the surface charge effect into account, and the measurements were intentionally performed slowly enough to suppress it.

Nonetheless, under the chosen conditions, the model was shown to estimate the PDIV reliably for four TPMW analogies with reduced coating thicknesses varying over an order of magnitude. The model's PDIV predictions are indeed valid over a broader range of reduced coating thicknesses as depicted in Figure 9. Compared to the predictions obtained specifically for the small reduced coating thickness ranges of each coating material, the values per the 'general model' have a maximum relative error of just 1.3 %.

B. Surface charge effect

As highlighted in Figure 8a, the PDIV/PDEV ratio showed different behavior depending on the material. The ratio was treated as a marker of the (PD-deposited) surface charge impact on the PD activity since the surface charge in particular should determine the PDIV-PDEV hysteresis. In general, the stronger the effect, the more the PD activity can be sustained below the original PDIV. By looking at the trends in Figure 8, one expects that the effect should be the strongest for PFA electrodes, followed by silicone polyester and unsealed alumina electrodes at approximately the same magnitude, whereas the effect should be the weakest for sealed alumina electrodes.

Since the employed geometry is comparable to the one of a cavity (gas gap delimited by insulation), the respective processes governing the surface charge dynamics shall be discussed briefly. In [16], these processes are listed: a migration and possible recombination of the surface charge due to surface conductivity, surface charge transport through the insulation bulk, and transition of the surface charge from shallow to deeper traps. Of these, the first two affect space charge distribution, whereas the third only affects starting electron generation through surface detrapping (further neglected due to the use of artificial UV illumination). Regarding the second

effect, the corresponding transport, or decay, is governed by the material time constant $\tau_{\mathrm{mat}} \approx \varepsilon/\sigma_{\mathrm{DC}}$. Even for the most conductive employed material, SA (Figure 3 σ_{DC}-lines), the material time constant would be in units of seconds, meaning that the decay of the surface charge through the insulation bulk would be negligible with respect to the employed test voltage frequencies.

Thus, only the migration of the surface charge appears to be relevant for the observed PDIV/PDEV behavior. Due to the employed geometry, where the two separate coating layers are in contact in a single point only, typically some hundreds of µm away from the discharge place (Figure 6), the recombination processes can be ruled out. By exclusion principle, only the surface charge migration hypothesis remains. This migration is driven by the tangential electric field (mostly created by the surface charge itself) and its speed is further determined by the surface conductivity. Since the location of the PD can be assumed to be the weak-point of the system when the test voltage is approximately equal to the PDIV, any migration of the surface charge from this place should be detrimental to sustaining the PD activity (PDIV/PDEV ratio should reduce). With the surface conductivity determining the migration's speed, its higher values should lead to lower PDIV/PDEV ratios.

By looking at Figure 3, one might expect the surface conductivity to be ordered as: SA $>$ UA $>$ SiPo $>$ PFA. When compared to the measured PDIV/PDEV ratios shown in Figure 8, the hypothesis seems to hold true, perhaps with a smaller difference between the ratios of UA and SiPo than expected. Moreover, an effect of surface charge shielding due to the difference between the value of ε_{r} at the PD timescale ($\approx$100 MHz) and at the test frequency could also explain the different PDIV/PDEV behavior. For the former, only the electronic and atomic polarization can be expected to be active, resulting in a lower value of ε_{r}; for the latter, the ε_{r} corresponds to the values shown in Figure 3. The higher the difference, the better the surface charge should be shielded, implying a weaker ability to sustain PD activity below the PDIV.

VI. Conclusion & Outlooks

The findings of this work can be summarized as follows:

- For room temperature, ambient pressure and zero relative humidity, the frequency dependence of the PDIV is exclusively determined via its indirect effect through the dielectric permittivity.
- The PDIV of the TPMW analogy test samples is accurately determined by the reduced thickness ($s/\varepsilon_{\mathrm{r}}$) of the samples' insulating coating.
- The accompanying breakdown model is shown to consistently provide reliable predictions of the PDIV over a broad range of reduced coating thicknesses, as experimentally verified for four different coating materials.
- An equation parametrizing the PDIV in the reduced coating thickness range of 1 µm to 50 µm is provided.
- The impact of discharge-deposited surface charge on the PD behavior is qualitatively described for the four materials using the PDIV/PDEV ratios and hypotheses based on the materials' dielectric characteristics are proposed.

Regarding future works, the next logical step would be to study the influence of one or more ambient conditions (gas density, temperature, relative humidity) to see if the proposed model still holds, i.e., whether the frequency dependence of the PDIV is still exclusively determined via its indirect effect on the reduced coating thickness. Furthermore, the proposed surface charge behavior hypotheses should be experimentally verified.

References

[1] A. Cavallini, "Reliability of low voltage inverter-fed motors: What have we learned, perspectives, open points," in *2017 International Symposium on Electrical Insulating Materials (ISEIM)*, vol. 1, 2017, pp. 13–22.

[2] R. Färber, T. Guillod, F. Krismer, J. W. Kolar, and C. M. Franck, "Endurance of polymeric insulation foil exposed to dc-biased medium-frequency rectangular pulse voltage stress," *Energies*, vol. 13, no. 1, p. 13, 2020.

[3] M. Kaufhold, G. Borner, M. Eberhardt, and J. Speck, "Failure mechanism of the interturn insulation of low voltage electric machines fed by pulse-controlled inverters," *IEEE Electrical Insulation Magazine*, vol. 12, no. 5, pp. 9–16, 1996.

[4] K. Wada, K. Tsuji, and H. Muto, "Partial discharge inception voltage for two insulating materials (PVC and PE) under inverter surge voltage," in *Proceedings of the 7th International Conference on Properties and Applications of Dielectric Materials (Cat. No.03CH37417)*, vol. 3, 2003, pp. 847–850 vol.3.

[5] D. R. Meyer, A. Cavallini, L. Lusuardi, D. Barater, G. Pietrini, and A. Soldati, "Influence of impulse voltage repetition frequency on rpdiv in partial vacuum," *IEEE Transactions on Dielectrics and Electrical Insulation*, vol. 25, no. 3, pp. 873–882, 2018.

[6] W. Pfeiffer and M. Paede, "About the influence of the frequency on the partial discharge characteristics of enamelled wires," in *Proceedings: Electrical Insulation Conference and Electrical Manufacturing and Coil Winding Conference (Cat. No.99CH37035)*, 1999, pp. 485–488.

[7] N. Hayakawa, F. Shimizu, and H. Okubo, "Estimation of partial discharge inception voltage of magnet wires under inverter surge voltage by volume-time theory," *IEEE Transactions on Dielectrics and Electrical Insulation*, vol. 19, no. 2, pp. 550–557, 2012.

[8] L. Lusuardi, A. Cavallini, M. G. de la Calle, J. M. Martínez-Tarifa, and G. Robles, "Insulation design of low voltage electrical motors fed by PWM inverters," *IEEE Electrical Insulation Magazine*, vol. 35, no. 3, pp. 7–15, 2019.

[9] K. Kimura, S. Ushirone, T. Fukushima, S. Ohtsuka, and M. Hikita, "Partial discharge inception voltage of twisted pair samples under long-time repetitive bipolar impulses," in *Conference Record of the 2004 IEEE International Symposium on Electrical Insulation*. IEEE, 2004, pp. 192–195. [Online]. Available: http://ieeexplore.ieee.org/document/1380514/

[10] K. Fukunaga, S. Okada, S. Ohtsuka, M. Hikita, and K. Kimura, "RPDIV/RPDEV characteristics of twisted-pair under repetitive bipolar impulse condition," in *2007 Annual Report - Conference on Electrical Insulation and Dielectric Phenomena*. IEEE, 2007, pp. 196–199. [Online]. Available: http://ieeexplore.ieee.org/document/4451612/

[11] K. Kimura, M. Hikita, N. Hayakawa, M. Nagata, K. Kadowaki, and Y. Murakami, "Round-robin test on repetitive PD inception voltage of twisted-pairs," in *2010 Annual Report Conference on Electrical Insulation and Dielectric Phenomena*, 2010, pp. 1–4.

[12] T. Kaji, H. Asai, H. Kojima, and N. Hayakawa, "Combined effect of temperature and humidity of magnet-wires on partial discharge inception voltage under inverter-surge voltage," in *2018 IEEE Conference on Electrical Insulation and Dielectric Phenomena (CEIDP)*, 2018, pp. 554–557.

[13] W. O. Schumann, *Elektrische Durchbruchfeldstärke von Gasen*. Springer, 1923.

[14] W. Rogowski, "Über Durchschlag und Gasentladung," *Zeitschrift für Physik*, vol. 100, no. 1, pp. 1–49, 1936.

[15] R. Dhariwal, J.-M. Torres, and M. Desmulliez, "Electric field breakdown at micrometre separations in air and nitrogen at atmospheric pressure," *IEE Proceedings-Science, Measurement and Technology*, vol. 147, no. 5, pp. 261–265, 2000.

[16] H. A. Illias, "Measurement and simulation of partial discharges within a spherical cavity in a solid dielectric material," Ph.D. dissertation, University of Southampton, May 2011. [Online]. Available: https://eprints.soton.ac.uk/194921/